J Mol Model (2013) 19:1417–1427
DOI 10.1007/s00894-012-1691-x

ORIGINAL PAPER

A theoretical investigation of the characteristics of hydrogen/halogen bonding interactions in dibromo-nitroaniline

Mehdi D. Esrafili

Received: 31 July 2012 / Accepted: 12 November 2012 / Published online: 8 December 2012
© Springer-Verlag Berlin Heidelberg 2012

Abstract In this work, computations of density functional theory (DFT) were carried out to investigate the nature of interactions in solid 2,6-dibromo-4-nitroaniline (DBNA). This system was selected to mimic the hydrogen/halogen bonding found within crystal structures as well as within biological molecules. DFT (M06-2X/6-311++G**) calculations indicated that the binding energies for different of interactions lie in the range between −1.66 and −9.77 kcal mol^{-1}. The quantum theory of atoms in molecules (QTAIM) was applied to provide more insight into the nature of these interactions. Symmetry-adapted perturbation theory (SAPT) analysis indicated that stability of the Br···Br halogen bonds is predicted to be attributable mainly to dispersion, while electrostatic forces, which have been widely believed to be responsible for these types of interactions, play a smaller role. Our results indicate that, for those nuclei participating in hydrogen/halogen bonding interactions, nuclear quadrupole resonance parameters exhibit considerable changes on going from the isolated molecule model to crystalline DBNA.

Keywords Halogen bond · σ-hole · Hydrogen bond · M06-2X · QTAIM · NQR

Electronic supplementary material The online version of this article (doi:10.1007/s00894-012-1691-x) contains supplementary material, which is available to authorized users.

M. D. Esrafili (✉)
Laboratory of Theoretical Chemistry, Department of Chemistry, University of Maragheh,
PO Box: 5513864596, Maragheh, Iran
e-mail: esrafili@fukui.kyoto-u.ac.jp

M. D. Esrafili
e-mail: esrafili@maragheh.ac.ir

Introduction

Protein folding, self-assembly, stacking of nucleobases, drug binding and crystal packing are all phenomena governed by noncovalent interactions [1–4]. Despite the central importance of such processes to chemistry, biology, and materials science, our current understanding of such underlying noncovalent interactions is far from complete. The hydrogen bond (HB), whose chief mode of interaction is through electrostatic and charge-transfer (delocalization) forces, has been the subject of many investigations and is believed to be the best characterized type of noncovalent interaction [5–9]. The HB is most frequently defined as an Y–H···Z interaction, where Y and Z are electronegative elements and Z possesses one or more lone electron pairs. However, there are also so-called unconventional HBs such as C–H···Y, Y–H···C, Y–H···π-electrons or even C–H···C [10]. However, increasing attention has been paid recently to other intermolecular interactions. Currently, halogen bonding [11–14] is becoming one of the most intensively investigated of such interactions, since it has been found to share many properties with HB. In fact, halogen bonding may be competitive to HB [15, 16] and, like HB, it may play a crucial role in stabilization of crystal structure [17, 18] and biomolecular systems [19, 20] and may also be useful in the design of new drugs and in material engineering [21, 22].

In the literature, halogen-bonding is usually explained in terms of the electrostatic potential on the surface of the halogen atom [23–26]. When a halogen X forms a covalent bond, which involves its half-filled *p* valence orbital, that electron is localized mainly in the bonding region, leaving a deficiency of electronic density in the outer (non involved) lobe of the *p*-type valence orbital, along the extension of the covalent bond to X. Through this positive region, which has been labeled a "*σ*-hole" [27], the halogen atom can interact

attractively with a negative site. Moreover, the positive region is frequently surrounded by a belt of negative electrostatic potential, which accounts for the possibility of interacting laterally with a positive site. Experimental results [28–30] and theoretical calculations [31–33] consistently show that the greater the polarizability and the lower the electronegativity of a halogen atom, the more positive is its σ-hole and the stronger is the halogen bond to which it gives rise. The strength of halogen bond formed by a halogen derivative with a given electron-rich moiety (halogen bond acceptor) thus decreases in the order I > Br > Cl. As a result of a combination of extreme electronegativity and limited polarizability, the F atom is frequently deemed to not participate in halogen-bonding. The electron density distribution around F is nearly spherical rather than anisotropic and, consequently, F is most likely to behave as a halogen bond acceptor. However, it has recently been shown that the fluorine atom has the capability of forming halogen bonds and can also affect recognition and self assembly processes, but only under specific circumstances [34, 35]. In this way, the interaction between halogen atoms and some negative charge concentration, e.g., a lone electron pair located on an oxygen or nitrogen atom, can be evident. Thus, halogen bonding is usually considered as an electrostatic interaction between the positive region on the halogen and a lone pair of a Lewis base [36, 37]. However, consideration of only the electrostatic interaction may not be sufficient to describe the ground-state stabilization of halogen bonding complexes. On the other hand, the contributions of polarization and dispersion also play an important role [38–40]. The relative contributions of these terms to attraction in halogen bonds varies from complex to complex. A recent study by Riley et al. [41] revealed that increasing the size and positive nature of a halogen's σ–hole markedly enhances the strength of the electrostatic component of the halogen bonding interaction. On the other hand, halogens with larger, more positive σ-holes tend to exhibit weaker dispersion interactions, which are attributable to the lower local polarizabilities of the larger σ-holes.

In a recent work, we reported several stable structures of dichloroacetic acid (DCAA) dimers in gas-phase [42]. This latter work, aimed at understanding the nature of interactions between DCAA monomers, focused on the properties of O–H···O, C–H···O, Cl···O and Cl···Cl interactions. An interesting finding was that, according to energy decomposition analysis, halogen bonds are largely dependent on both electrostatic and dispersion interactions. In the current study, we worked towards a more complete understanding of the hydrogen/halogen bonding interactions by studying the electronic structure of 2,6-dibromo-4-nitroaniline (DBNA) in solid phase (Fig. 1). This system was selected to mimic the halogen bonding found within crystal structures as well as within biological molecules. Such a theoretical study may provide some valuable information of the origin and strength of halogen bonding interactions, which would be very important for the design and synthesis of new materials and effective drugs containing halogenated compounds.

Computational details

All density functional theory (DFT) calculations were performed using the GAMESS electronic structure package [43]. The X-ray crystalline structures of DBNA were available from [44]. Since the positions of hydrogen atoms are not located accurately by X-ray diffraction, a geometry optimization of just the hydrogen atoms in the structure was needed. In the present study, partial geometry optimizations were carried out using B3LYP, M06-2X, TPPSh functionals with 6-311 + G* standard basis set. According to Zhao and Truhlar [45–48], the M06 series of functionals implicitly account for "medium-range" electron correlation because of the way they are parametrized, and this is sufficient to describe the dispersion interactions within many complexes [48]. These authors define "medium-range" correlation to be that found in complexes separated by about 5 Å or less [49]. While initial tests of these functionals have been very promising [50], they have yet to be fully benchmarked for biologically relevant noncovalent interactions.

Electrostatic surface potentials were calculated at M06-2X/6-311++G** level using WFA program [51]. The quantum theory of atoms in molecules (QTAIM) [52] analysis was preformed with the help of AIM 2000 software [53] using the wave functions generated at the M06-2X/6-311++G** level. To shed more light on the nature of the hydrogen/halogen bond, we also performed decomposition of the interaction energy by means of the symmetry-adapted perturbation theory (SAPT) method [54] with the use of the Dalton 2.0 package [55] interfaced to the SAPT2008 code [56]. In this study, we employed so-called SAPT2 approximation to the intermolecular interaction energy. The interaction energy at the SAPT2 level is defined as follows:

$$E_{int}^{SAPT2} = E_{elst}^{(10)} + E_{exch}^{(10)} + E_{ind,resp}^{(20)} + E_{exch-ind,resp}^{(20)} + E_{disp}^{(20)} + E_{exch-disp}^{(20)} + E_{elst,resp}^{(12)} + {}^{t}E_{ind}^{(22)} + {}^{t}E_{exch-ind}^{(22)} + E_{exch}^{11} + E_{exch}^{12} + \delta E_{int,resp}^{(HF)} \quad (1)$$

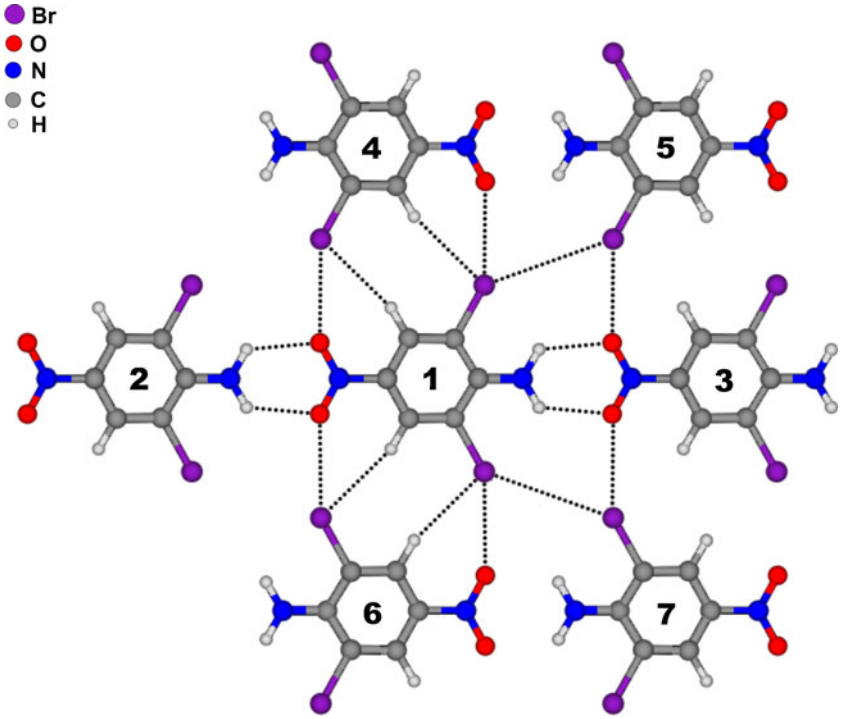

Fig. 1 Intermolecular interactions in crystalline structure of 2,6-dibromo-4-nitroaniline (DBNA). *Dotted lines* Hydrogen/halogen bonding interactions

where

$$\delta E^{HF}_{int,resp} = E^{HF}_{int} - E^{(10)}_{elst} - E^{(10)}_{exch} - E^{(20)}_{ind,resp} - E^{(20)}_{exch-ind,resp} \quad (2)$$

The right side of Eq. (1) is a sum of perturbative energy correction terms that are the consequences of various physical interaction forces. These energy correction terms, except for the very last one, were collected into four fundamental physical components: electrostatic (E_{elst}), exchange (E_{exch}), induction (E_{ind}), and dispersion (E_{disp}) as follows:

$$E_{elst} = E^{(10)}_{elst} + E^{(12)}_{elst,resp} \quad (3)$$

$$E_{exch} = E^{(10)}_{exch} + E^{(11)}_{exch} + E^{(12)}_{exch} \quad (4)$$

$$E_{ind} = E^{(20)}_{ind,resp} + {}^{t}E^{(22)}_{ind} + E^{(20)}_{exch-ind,resp} + {}^{t}E^{(22)}_{exch-ind} \quad (5)$$

$$E_{disp} = E^{(20)}_{disp} + E^{(20)}_{exch-disp} \quad (6)$$

The above grouping scheme in SAPT2 analysis is used because it was indicated that such a scheme is more appropriate and easier to interpret than other possible schemes [57].

In nuclear quadrupole resonance (NQR) spectroscopy, the interaction between nuclear electric quadrupole moment and electric field gradient (EFG) at quadrupole nucleus is described with Hamiltonian as follows [58]:

$$\hat{H} = \frac{e^2 Q q_{zz}}{4I(2I-1)}\left[\left(3\hat{I}_z^2 - \hat{I}^2\right) + \eta_Q\left(\hat{I}_x^2 - I_y^2\right)\right] \quad (7)$$

where eQ is the nuclear electric quadrupole moment, I is the nuclear spin, and q_{zz} is the largest component of the EFG tensor. The principal components of the EFG tensor, q_{ii}, are computed in atomic unit ($1\ au = 9.717365\times10^{21} V\,m^{-2}$), with $|q_{zz}|\geq|q_{yy}|\geq|q_{xx}|$ and $q_{xx}+q_{yy}+q_{zz}=0$. These diagonal elements relate to each other by the asymmetry parameter: $\eta_Q=|q_{yy}-q_{xx}|/|q_{zz}|$, $0\leq\eta_Q\leq1$, that measures the deviation of EFG tensor from axial symmetry. The computed q_{zz} component of EFG tensor is used to obtain the nuclear quadrupole coupling constant from the equation; $C_Q(\mathrm{MHz})=e^2Qq_{zz}/h$, using the recently reported value for the ^{2}H,^{14}N, ^{79}Br and ^{17}O electric quadrupole moments of 2.86, 20.44, −313 and −25.58 mb, respectively [59].

Results and discussion

The present study investigates the properties of conventional N–H···O and unconventional C–H···Br, Br···Br and Br···O types of intermolecular interactions in crystalline structures of DBNA. We looked in detail at the electrostatic potential

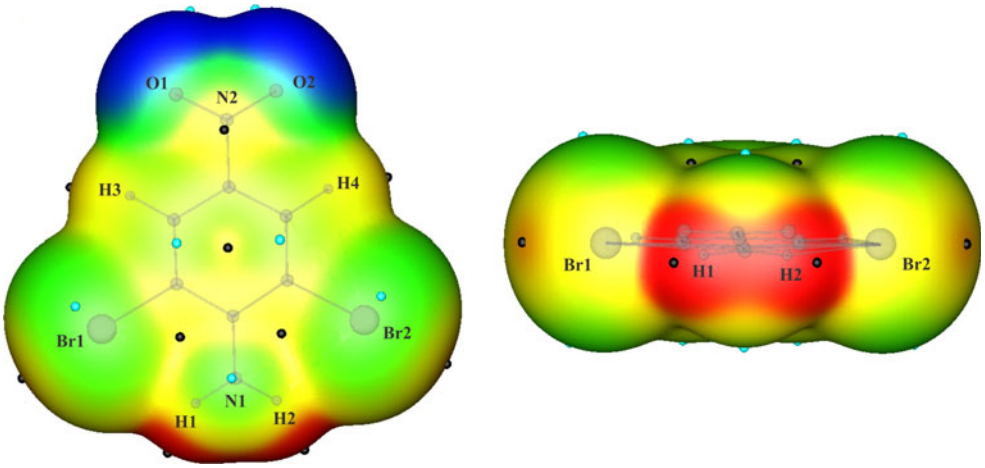

Fig. 2 Electrostatic potential mapped on the surface of DBNA molecular electron density (0.001 e au^{-3}). Color ranges for $V_{S(r)}$, in kcal mol^{-1}: *red* >26.5, *yellow* 26.5–5.7, *green* 5.7– −15.1, *blue* < −15.1. *Black circles* Surface maxima, *blue* surface minima

on the surface of monomer DBNA, and at the electrostatically driven noncovalent bonds that can be formed between atoms (Fig. 2). To gain further insights into the nature of these intermolecular interactions, the QTAIM and SAPT energy decomposition analysis were used (Tables 1, 2). To include hydrogen/halogen bonding interactions effects, EFG calculations were performed for two molecular models including the monomer and seven-molecule cluster. To the best of our knowledge, no experimental NQR data have been reported on DBNA. Thus, the calculated NQR parameters of DBNA were compared with the available experimental NQR data. Unless otherwise noted, results refer to the M06-2X/6-311++G** level of theory.

Surface electrostatic potential

The electrostatic potential V(r) that the electrons and nuclei of a molecule create at any point r is given rigorously by Eq. (8):

$$V(r) = \sum_A \frac{Z_A}{|R_A - r|} - \int \frac{\rho(r')dr'}{|r' - r|} \tag{8}$$

in which Z_A is the charge on nucleus A, located at R_A, and ρ(r) is the molecule's electronic density. V(r) is a physical observable quantity; it can be obtained experimentally by diffraction methods [60] as well as computationally. The analysis of V(r) has proven to be an effective approach to interpreting and quantifying noncovalent interactions [61] that are primarily electrostatic in nature. For this purpose, we compute V(r) on the molecular "surface", which we define, following Bader et al. [62], as the 0.001 electrons/bohr^3 contour of the electronic density ρ(r). This surface potential is labeled V_S(r).

Figure 2 displays the evaluated V_S(r) on the 0.001 au surface of DBNA. The figure shows the locations of the various most positive and most negative V_S(r), designated $V_{S,max}$ and $V_{S,min}$. As would be anticipated, there is a strong

Table 1 Hydrogen/halogen bond distances, and topological parameters of electron density for crystalline 2,6-dibromo-4-nitroaniline (DBNA) calculated at the M06-2X/6-311++G** level of theory. All ρ_{BCP}, $\nabla^2\rho_{BCP}$, G_{BCP}, V_{BCP} and H_{BCP} parameters in 10^3 au

Interaction	Distance	ρ_{BCP}	$\nabla^2\rho_{BCP}$	G_{BCP}	V_{BCP}	H_{BCP}	ε
O1(1)···H1(2)	2.225	14.55	56.36	12.05	−10.00	2.04	0.01
O2(1)···H2(2)	2.225	14.55	56.37	12.05	−10.00	2.05	0.01
O1(1)···Br2(4)	3.218	7.65	29.50	6.21	−5.04	1.17	0.05
H3(1)···Br2(4)	3.036	5.66	16.27	3.29	−2.52	0.77	0.07
Br1(1)···H4(4)	3.034	5.69	16.27	3.29	−2.50	0.78	0.08
Br1(1)···O2(4)	3.218	7.64	29.29	6.17	−5.01	1.16	0.05
Br1(1)··· Br2(5)	4.192	2.60	8.23	1.51	−0.96	0.55	0.20
H1(1)··· O1(3)	2.227	14.40	55.96	11.95	−9.90	2.04	0.01
H2(1)··· O2(3)	2.227	14.40	55.96	11.95	−9.90	2.04	0.01
Br2(1)··· Br1(7)	4.192	2.60	8.23	1.51	−0.96	0.55	0.20
Br2(1)··· O2(6)	3.218	7.64	29.30	6.17	−5.01	1.16	0.05
Br2(1)··· H3(6)	3.034	5.70	16.27	3.29	−2.50	0.78	0.08
H4(1)···Br1(6)	3.036	5.66	16.27	3.29	−2.52	0.77	0.07
O2(1)···Br1(4)	3.219	7.65	29.50	6.21	−5.04	1.17	0.05
H1(1)···Br1(1)	2.613	15.05	61.37	12.89	−10.43	2.45	2.59
H2(1)···Br2(1)	2.613	15.05	61.34	12.88	−10.43	2.45	2.56

Table 2 Calculated interaction energies and symmetry-adapted perturbation theory (SAPT) decomposition analysis of DBNA dimers. All basis set superposition error (BSSE) corrected interaction energies and energy components were calculated using 6-311++G** basis set and in kcal mol^{-1}

Dimer	E_{int}^{HF}	E_{int}^{MP2}	E_{int}^{M06-2X}	E_{int}^{B3LYP}	E_{int}^{TPSSh}	E_{int}^{SAPT2}	E_{elst}	E_{exch}	E_{ind}	E_{disp}
No.1···No.2	−6.57	−9.77	−9.32	−7.28	−7.42	−10.12	−22.84	18.13	−3.68	−2.45
No.1···No.3	−6.55	−9.75	−9.30	−7.24	−7.38	−10.11	−22.84	18.13	−3.68	−2.45
No.1···No.4	−5.77	−11.98	−9.77	−6.75	−7.04	−12.70	−12.39	10.2	−4.13	−5.88
No.1···No.5	−0.95	−2.49	−1.66	−0.90	−1.19	−2.68	−1.35	1.98	−0.91	−2.35
No.1···No.6	−5.76	−11.97	−9.76	−6.74	−7.03	−12.69	−12.39	10.2	−4.13	−5.88
No.1···No.7	−0.93	−2.50	−1.67	−0.90	−1.19	−2.68	−1.35	1.98	−0.91	−2.34

positive potential encompassing the amine hydrogens, with $V_{S,max}$=+47.4 kcal mol^{-1}. Perhaps more surprisingly there is also a smaller and weaker positive region on the outermost portion of each bromine, centered about the intersection of its surface with the C–Br axis. These $V_{S,max}$ are +24.6 kcal mol^{-1}. Such halogen-positive regions, which have been given the name "σ-holes", are found on some covalently bonded chlorines, but more often (and more positive) on bromines and iodines [11–14]. They have been invoked as the explanation for "halogen bonding"—a noncovalent interaction (somewhat analogous to HB) between a covalently bound halogen on one molecule and a negative site on another. It is the presence of a positive σ-hole that is believed to make this possible.

From Fig. 2, it is evident that the most negative electrostatic potential on the DBNA surface is associated with the nitro oxygens, $V_{S,min}$=−35.9 kcal mol^{-1}. These are located in the NO_2 plane and can be attributed to the overlapping electronic densities of the two oxygen unshared electrons pairs. On the other hand, the very strongly positive electrostatic potential of the amino hydrogen, $V_{S,max}$=+47.4 kcal mol^{-1}, and the $V_{S,min}$=−35.9 kcal mol^{-1}of the nitro oxygen indicate their propensities for noncovalent HB, as a donor and an acceptor, respectively. Moreover, the C-H···Br interaction seems to be weaker than the N–H···O interaction, because the hydrogen atom of the former has a less positive electrostatic potential; $V_{S,max}$=+21.7 kcal mol^{-1} in H3 or H4 vs +47.4 kcal mol^{-1} in H1 or H2. In crystalline DBNA, it can be seen that one of the positive $V_{S(r)}$ regions on the bromine of the target molecule, along the extension of the C–Br bond, is interacting with the negative potential on the side of the bromine atoms of neighbor molecules (see Figs. 1 and 2). The evaluated Br···Br separation is 4.192 Å. These separations are slightly longer than the sum of two chlorine van der Waals (vdW) radii, 3.70 Å [63]. However, it should be pointed out that not all halogens with positive σ–hole potentials have negative lateral sides. There are a number of computational treatments [31, 33] of covalently-bonded R-X systems that indicate the interaction energies for forming a single donor–acceptor complex R–X···X become less negative as the electron-withdrawing capacity of R increases and, for a given R, on going from X, is F to Cl to Br to I. Thus, for the X–CN molecule, the key to the positive lateral is apparently the very strong electron-attracting power of the CN substituent, both through resonance, and inductively. This results in the halogen surface being completely positive. Therefore, it may be concluded that the weakness of the Br···Br interactions in solid DBNA can be rationalized by looking at the general range of negative potential values on the lateral sides of the bromines (−1.1 to −1.5 kcal mol^{-1}) compared to, for example, the negative potentials of the nitro oxygens (−35.9 kcal mol^{-1}).

As shown in Fig. 2, the evaluated electrostatic potential shows the presence of a slightly positive potential end cap and a negative region on the side of the Br atoms ($V_{s,max}$= +24.6 kcal mol^{-1}). The positive region on the extension of each C–Br bond interacts with the negative potential on the nitro oxygens (see Fig. 1). The Br···O bonds are slightly less than the sum of the vdW radii of the Br and O atoms (3.37 Å) [63], implying an attractive interaction between DBNA monomers. For such an interaction, the positive region on the extension of C–Br bond of target molecule (with $V_{S,max}$= +24.6 kcal mol^{-1}) is interacting with the negative potential on the oxygen of the neighbor molecule (with $V_{S,min}$= −35.9 kcal mol^{-1}, see Figs. 1 and 2).

Local topological analysis

Topological analysis of the electron density constitutes an insightful tool to investigate the electronic properties of molecular systems and allows a deep examination of the interatomic interactions. In addition, this methodology has been applied successfully in the study of the properties of a variety of conventional and unconventional HBs [64, 65] as well as of the halogen bonds [13, 14]. Based on the QTAIM theory, the electron density (ρ), its Laplacian ($\nabla^2\rho$) and electronic energy density (H_{BCP}) at a bond critical point (BCP) give us information about the strength and characteristic of the bond [52]. The electronic energy density is obtained from the equation $H_{BCP}=G_{BCP}+V_{BCP}$, where G_{BCP} and V_{BCP} are the local kinetic and potential energy densities, respectively. The energy density term

G_{BCP} is calculated based on equation $(1/4)\nabla^2\rho_{BCP}=2G_{BCP}+V_{BCP}$.

Results concerning relevant QTAIM parameters calculated at the BCPs of N–H···O, C–H···Br, Br···Br and Br···O bonds are given in Table 1 and Tables S1 and S2 (Supporting Information). For the N–H···O interactions, it can be seen that the values of ρ_{BCP} are calculated to be 0.014 au, whereas the values of $\nabla^2\rho_{BCP}$ are positive (0.056 au). These values are within the commonly accepted values for H-bonding interactions, thus indicating the closed-shell interactions in DBNA. However, positive values of H_{BCP} are predicted for these HBs, suggesting that the interactions are mainly electrostatic in nature, and therefore a relatively large ionic contribution is necessarily invoked. This proposal is supported by results from an energy decomposition analysis of DCAA dimers [42]. As is obvious from Table 1, the ellipticity values for the two N–H···O interactions are very small or zero, indicating that the HBs are conserved in the solid DBNA. The topological values of the C–H···Br interaction in crystalline DBNA are also listed in Table 1. Relatively small values of ρ_{BCP} (0.006 au), the positive values of the Laplacian, and values of $H_{BCP}>0$, guarantee the existence of a weak H-bonding.

Earlier studies have established that a partly covalent interaction can be said to exist if $\nabla^2\rho_{BCP}$ is positive and H_{BCP} is negative [66]. An alternative tool for assessing the nature of hydrogen/halogen bond is the ratio $-G_{BCP}/V_{BCP}$. Accordingly, if $-G_{BCP}/V_{BCP}>1$, then the interaction is noncovalent in nature. On the other hand, if $0.5<-G_{BCP}/V_{BCP}<1$ then the interaction is partly covalent. From Table 1, despite falling in a region of charge depletion with $\nabla^2\rho_{BCP}>0$, the all Br···Br BCPs are characterized by a positive H_{BCP} value and $-G_{BCP}/V_{BCP}>1$, indicating that the kinetics energy overcomes the potential energy density at the BCP and that the Br···Br bonds are noncovalent in nature. As is obvious from Table 1, the small values of ρ_{BCP}, the positive values of the $\nabla^2\rho_{BCP}$ and the nearly zero values of H_{BCP} suggest, according to the Rozas [66] criterion, that all Br···O intermolecular interactions are weak and basically electrostatic in nature. More specifically, it can be seen that the values of ellipticity obtained for the Br···O interactions are small (0.05), thus revealing the stability of the Br···O bonds. This finding is in agreement with the evaluated electrostatic potential results mentioned above.

From Fig. 1, it is evident that the orientation of the amine hydrogens with respect to the C–Br bond favors a linear arrangement. Values of the C–Br···H and N–H···Br angles, together with coplanarity of these bonds, correspond to orientation of the σ-holes of the amine hydrogen atom toward one of the lone pairs of the bromine atom. The bonding character of the intramolecular N–H···Br interaction is confirmed unambiguously by the presence of BCP and the bond path between these atoms (Fig. 3). Both of these topological features thus suggest stabilizing the attractive nature of the N–H···Br interaction. On inspecting the values of QTAIM parameters computed for the BCP of this interaction (see Table 1), one could conclude that it is of the closed-shell type as indicated by low values of electron density (0.015 au) and positive values of both its Laplacian and the electronic total energy density (0.002 au). This reflects the weak character of the N–H···Br interaction, which is comparable with the N–H···O hydrogen bonds. This conclusion is confirmed also by values of $V_{S(R)}$ derived from surface electrostatic potential analysis. It has been shown, however, that the intramolecular N–H···Br interaction is characterized by the relative unusually large value of ε, thus indicating a topological instability.

Interaction energies and SAPT analysis

As already mentioned in the literature, the hydrogen/halogen bond is most often believed to be electrostatic in nature, although the relevance of other energy contributions has also been shown [39–42, 67, 68]. The nature of the Br···Br bond has been investigated only rarely. Although decompositions of the halogen bonding interaction have been investigated [38–42], none of these decompositions has been examined for the crystalline phase. Thus, for all DBNA dimers investigated in this study, we performed SAPT2 analysis and compared the evaluated SAPT2 interaction energies with those obtained by HF, M06-2X, B3LYP, TPSSh and MP2 methods (Table 2). Estimation of the basis set superposition error (BSSE) for all of the structures presented here was performed by the full counterpoise method [69].

Let us first analyze BSSE-corrected interaction energies (E_{int}). Table 2 lists the calculated interaction energies obtained with the HF, MP2, B3LYP, M06-2X, TPSSh and SAPT methods for the various DBNA dimers. From Table 2, the most important finding is that the values of the interaction energies depend appreciably on the method used and/or the dimer considered. First, it is evident that E_{int}^{HF} is always smaller in magnitude than the others. A more detailed analysis of these results shows that, in general, the MP2 method provides larger stabilization energy than the others. Considering the MP2 results, it is evident that inclusion of correlation reproduces stabilization of complexes as high as 1.54–6.21 kcal mol^{-1}. As can be seen, the HF method greatly underestimates the interaction energies of the complexes and, in the case of halogen-bonded No1···No5 dimer, predicts a small binding energy of −0.95 kcal mol^{-1}. This indicates that dispersion must play a significant role in the stabilization of DBNA monomers. Previous publications [70, 71] indicated that the difference between MP2 and HF energies is attributed mainly to the effects of high-order electrostatic interaction. Consequently, due to the significant gain in attraction by electron correlation (1.54–6.21 kcal mol^{-1} at MP2 level), dispersion force plays a

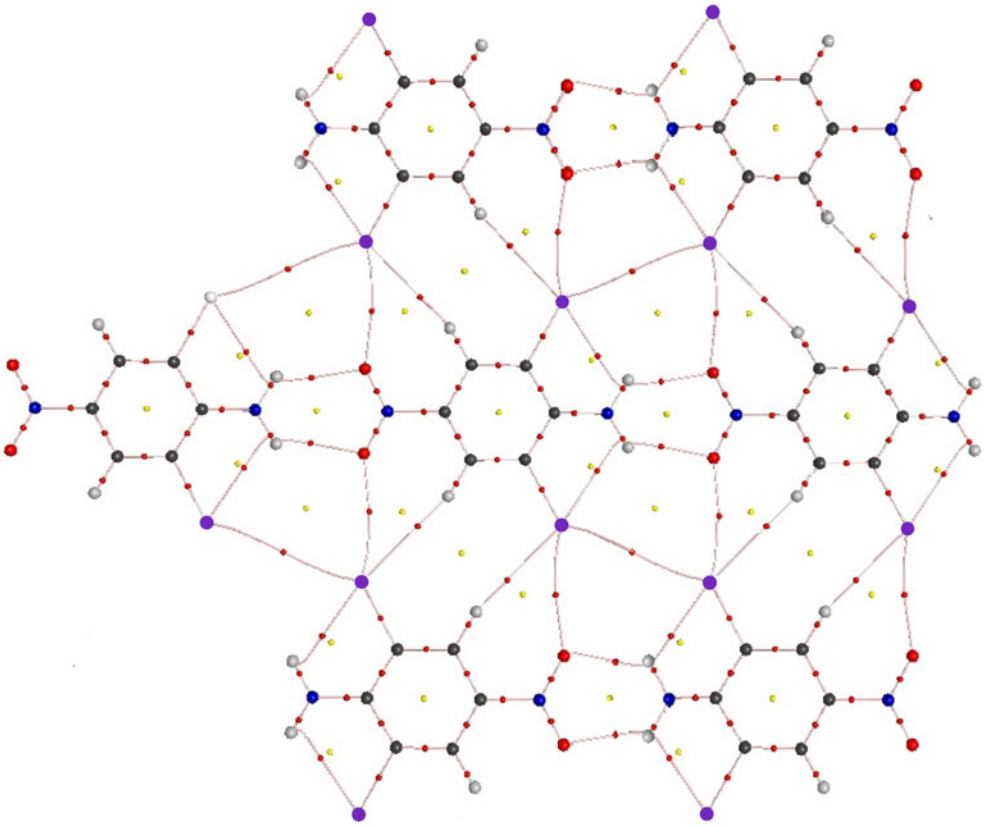

Fig. 3 Molecular graphs of crystalline DBNA. *Solid lines* Bond paths, *large circles* attractors, *small red circles* bond critical points (BCPs)

considerable role in the stability of the dimers. The results in Table 2 indicate that the interaction energies predicted by the B3LYP functional are lower by 1.59−5.23 kcal mol^{-1} in comparison with the MP2 method. This is due to the fact that about 40 % of the short-range dispersion energy is neglected by the B3LYP functional [72].

Before we take a look at the individual contributions to the intermolecular energy, we shall discuss the accuracy of the SAPT2 results. From Table 1, it is evident that the SAPT2 binding energies are all slightly higher than those of MP2 as computed using the 6-311++G** basis set, and that the difference between MP2 and SAPT energies increases as the interaction between the DBNA monomers becomes more negative. As in the supermolecular results, the No.1···No.4 is the most stable complex (−12.70 kcal mol^{-1} at the SAPT2 level). Table 2 also indicates that the SAPT2 interaction energies for the DBNA dimers are generally in good agreement with those obtained using the M06-2X and TPSSh methods, suggesting that SAPT is an appropriate method to study the intermolecular interactions in these studied complexes. The calculated SAPT2 binding energy for the halogen-bonded No.1···No.5 complex is −2.68 kcal mol^{-1}, which overestimates MP2 energies by about 0.19 kcal mol^{-1}.

To better understand the nature and the extent of different forces contributing to intermolecular attraction in crystalline DBNA, individual energy components of the total interaction energy were obtained using SAPT2. It should be noted here that, although the most frequently quoted mechanism of halogen bond formation may suggest a significantly electrostatic nature of this interaction [38–42], the Kohn–Sham molecular orbital approach indicates the significantly covalent character of such interaction [14]. However, in some cases, the resulting interpretations between interaction energy terms may be contradictory. For instance, based on the SAPT decomposition method, the formation of F_3C–Cl···O=CH_2, F_3C–Br···O=CH_2 and F_3C–I···O=CH_2 complexes, are attributed primarily to electrostatic and dispersion effects [37], while the method proposed by Palusiak [14], for exactly the same interactions, concludes that charge transfer and polarization dominate, with electrostatics contributing only "slightly". On the other hand, on the basis of binding energy decomposition of halogen-bonded complexes, Politzer et al. [73] indicated that the formation and observed properties of the resulting noncovalent complexes can be fully explained in terms of electrostatics/polarization plus dispersion as the driving forces.

The electrostatic component of the interaction energy is represented here by the sum of $E_{elst}^{(10)}$ and $E_{elst,resp}^{(12)}$ terms (Table 2). From Table 2, it is evident that for the N–H···O, C–H···Br and Br···O interactions, the most stabilizing interaction energy component is the electrostatic one. However, for the No.1···No.5 dimer (Br···Br interaction), the exchange

energy becomes even larger than the absolute value of the electrostatic energy, but the large attractive induction and dispersion energies lead to a stabilizing interaction. From Table 2, it is found that all contributions of the electrostatic, induction and dispersion terms have a stabilizing effect. For the H-bonded dimers, the major contribution is the electrostatic interaction energy, which presents between 55 % and 78 % of the total stabilization energy. Considering the SAPT2 results, it is also found that the electrostatic effects account for about 78 % of the overall attraction in the N–H···O H-bonded dimer. By comparison, the induction component of this interaction represents about 14 % of the total attractive forces, while dispersion contributes 8 % to the stability of this structure. Thus it can be said that the N–H···O interaction is remarkably dependent on both electrostatic and induction forces, with electrostatic forces playing the largest role in their stability. In contrast, the stabilities of Br···Br halogen bonds are predicted to be attributable mainly to dispersion (50 %), while electrostatic forces, which have been widely believed to be responsible for these types of interactions, play a smaller role (29 %).

NQR parameters

As seen in previous section, $V_{S(r)}$ analyses have shown that DBNA offers a remarkable array of possible sites for intermolecular electrostatic interactions, foremost of which are the strongly negative nitro oxygens. In addition, the bromine atoms in DBNA have a significant negative region (Fig. 2). On the positive side must be considered the amine hydrogens. Table 3 shows the effects of HBs and halogen bonds interactions on the C_Q and η_Q parameters at the sites of ^{79}Br, ^{17}O, ^{14}N and ^{2}H nuclei of DBNA. NQR parameters were evaluated using the M06-2X, B3LYP, and TPSSh density functionals with 6-311++G** basis set. It is evident that the C_Q values obtained by different DFT methods are in agreement with each other to within 0.52–0.86 MHz, 0.16–0.59 MHz, 3.29–15.28 MHz and 0.94–7.23 KHz for the ^{17}O,^{14}N, ^{79}Br and ^{2}H nuclei, respectively. In the cases of ^{17}O and ^{2}H nuclei, the M06-2X functional slightly overestimates the evaluated C_Q values, as compared to the others (Table 3). On the other hand, B3LYP predicts the largest C_Q parameter for ^{79}Br nuclei.

In crystalline DBNA [44], weak HBs exist between the pair of amino hydrogens on one molecule and the pair of p-nitro oxygen atoms on an adjacent molecule (Fig. 1). A quick look at the results reveals that intermolecular N–H···O interactions affect the calculated ^{17}O NQR parameters at the sites of O1 and O2; however, such an influence is exactly equivalent for the two oxygen nuclei. As seen in Table 3, M06-2X calculations reveal that the $C_Q(^{17}O)$ parameter decreases by 0.55 MHz depending on whether the DBNA molecule is in the gas phase or in a crystal lattice. On the other hand, the corresponding asymmetry parameter increases about 0.08 units on going from the single monomer to the target molecule in the cluster. Figure 1 also indicates that the two bromine atoms Br1 and Br2 occupy somewhat the same position in the crystalline state of DBNA. The variation in the calculated $C_Q(^{79}Br)$ parameters for these sites can be fully explained in terms of the changes in the corresponding Br···Br, C−H···Br and Br···O bond distances between the two models. The M06-2X calculations reveal that $C_Q(^{79}Br)$ at the site of the bromine atoms increases by 8.17 MHz from the monomer to the target molecule in the cluster (Table 1). Besides, the corresponding η_Q value at this site increases from 0.02 units (monomer) to 0.03 units (cluster).

In common with previous works [6, 7], N–H···O interactions make significant changes to the calculated ^{14}N

Table 3 Calculated nuclear quadrupole resonance (NQR) parameters of crystalline DBNA. C_Q values for ^{17}O, ^{14}N and ^{79}Br nuclei are in MHz, those for ^{2}H in kHz. For each nucleus, the value in parenthesis refers to the gas phase DBNA monomer, while the other is for the target molecule in crystalline phase

Nucleus	M06-2X		B3LYP		TPSSh	
	C_Q	η_Q	C_Q	η_Q	C_Q	η_Q
^{17}O1	14.03 (14.58)	0.69 (0.61)	13.50(14.10)	0.77(0.66)	13.16(13.79)	0.78(0.68)
^{17}O2	14.03 (14.59)	0.70 (0.62)	13.51(14.11)	0.77(0.67)	13.17(13.80)	0.79(0.68)
^{79}Br1	566.86 (558.69)	0.03 (0.02)	582.13(570.81)	0.05(0.03)	570.15(559.33)	0.04(0.03)
^{79}Br2	567.10 (558.97)	0.03 (0.02)	582.38(571.09)	0.05(0.03)	570.40(559.60)	0.04(0.03)
^{14}N1	3.80 (4.49)	0.36 (0.23)	3.87(4.63)	0.34(0.21)	3.85(4.59)	0.32(0.19)
^{14}N2	1.76 (−1.47)	0.81 (0.98)	1.33(1.10)	0.13(0.34)	1.17(0.96)	0.29(0.11)
^{2}H1	265 (277)	0.18 (0.20)	260(271)	0.18(0.21)	258(269)	0.17(0.20)
^{2}H2	265 (277)	0.18 (0.20)	261(271)	0.18(0.21)	258(269)	0.17(0.20)
^{2}H3	210 (212)	0.05 (0.04)	209(209)	0.05(0.05)	210(210)	0.05(0.04)
^{2}H4	210 (212)	0.05(0.04)	209(209)	0.05(0.05)	210(210)	0.05(0.04)

NQR parameters. As Fig. 1 indicates, there are two crystallographically distinct nitrogen sites in DBNA [44]: amine $^{14}NH_2$, and nitro $^{14}NO_2$. From Table 3, it can be seen that all of the $C_Q(^{14}N)$ values of the monomer DBNA lie within the −1.47–4.63 MHz and that of $^{14}NO_2$ is relatively lower than $^{14}NH_2$. Evidently, different C_Q and η_Q values observed for the nitrogen sites in the monomer DBNA must arise from differences in the surrounding environment. A quick look at the results reveals that intermolecular hydrogen/halogen bonding interactions affect the calculated ^{14}N NQR parameters at the N1 and N2 sites; however, such an influence is not equivalent for the two nitrogen nuclei. Table 3 indicates that variation in the calculated NQR parameters of N2 between the two molecular models is more significant than for N1, with differences of up to 3.23 MHz and 0.17 units for $C_Q(^{14}N)$ and the magnitude of the asymmetry parameter, respectively. In contrast, the NQR parameters for N1 show less sensitivity to hydrogen/halogen bonding. Figure 1 indicates that N1 contributes to the N–H···O as well as intramolecular N–H···Br H-bonding interactions in crystalline DBNA. Because of the proper H-bonding distances, C_Q(N1) decreases by 0.69 MHz from the monomer to the target molecule in the cluster. The η_Q parameter increases by 0.13 units from the monomer to the cluster. The calculated C_Q and η_Q parameters for N1 in crystalline DBNA is 3.80 MHz and 0.36 units, which differ slightly from those of crystalline aniline (exp. 3.933 MHz and 0.27 units) [74].

As mentioned above, the positive $V_{S(r)}$ region on the amine hydrogens is interacting with the negative potential on the side of the nitro oxygens and bromine atoms. It thus seems justified to describe the formation of these interactions as electrostatically driven. Table 3 summarizes the calculated and reported experimental NQR parameters of the amine hydrogen atoms (H1 and H2). Due to the HBs, the C_Q (^2H) value at the NH_2 site undergoes a significant change from the monomer to the target molecule in the cluster. More specifically, M06-2X/6-311++G** calculations reveal that NQR parameters at this site vary considerably between the monomer and octamer cluster, ΔC_Q =12 kHz and $\Delta\eta_Q$=0.02 units. The calculated C_Q and η_Q values for the H1 and H2 of the target molecule are obtained to be 265 kHz and 0.18 units, respectively. These values, which are obtained by taking the whole cluster into consideration, are expected to be close to that of aniline (C_Q= 236 MHz and η_Q=0.18 units) [75]. From Fig. 1, it is clear that molecules No. 4 and 6 are capable of making a weak C–H···Br interactions with the target molecule, $r_{C\text{-}H3\cdots Br}$=3.036 Å, ∠ C-H···Br=164°. Because of the unusual nature of the C–H···Br interaction in biological systems, it is therefore of interest to examine the effect of this interaction on the ^2H NQR parameters in more detail. However, as the results of Table 3 illustrate, including the C–H···Br type H-bonding interaction decreases the calculated $C_Q(^2H)$ by 2 kHz and increases the η_Q value by 0.01 units. This is due to the limited involvement of this group in the intermolecular interaction of crystalline DBNA.

Summary

In summary, we have systematically investigated the hydrogen/halogen bonding interaction in crystalline DBNA. We also focused on the decomposition of the interaction energy into physically meaningful terms and characterized and described the intermolecular interaction on the basis of the parameters of molecular properties. Our results can be summarized as follows:

(1) The results of surface electrostatic potential analysis revealed that there is a strong positive potential encompassing the amine hydrogen, with $V_{S,max}$= +47.4 kcal mol^{-1}. Moreover, there is also a smaller and weaker positive region on the outermost portion of each bromine, centered about the intersection of its surface with the C–Br axis.

(2) The small values of ρ_{BCP}, the positive values of the $\nabla^2\rho_{BCP}$ and the nearly zero values of H_{BCP} suggest that the all N–H···O, C−H···Br and Br···O intermolecular interactions are weak and basically electrostatic in nature.

(3) This study found that the values of the interaction energies depend considerably on the method used and/or the dimer considered. A more detailed analysis of these results shows that, in general, the MP2 method provides larger stabilization energy than the others.

(4) It is found that SAPT2 binding energies are all slightly higher than those of MP2 as computed using the 6-311++G** basis set, and that the difference between MP2 and SAPT energies increases as the interaction between the DBNA monomers becomes more negative.

(5) From SAPT analysis, it is concluded that for the N–H···O, C–H···Br and Br···O interactions, the most stabilizing interaction energy component is the electrostatic one. However, for the Br···Br interaction, the exchange energy becomes even larger than the absolute value of the electrostatic energy, but the large attractive induction and dispersion energies lead to a stabilizing interaction. The stabilities of the Br···Br halogen bonds are predicted to be attributable mainly to dispersion (50 %), while electrostatic forces, which have been widely believed to be responsible for these types of interactions, play a smaller role (29 %).

(6) Our results indicate that NQR parameters of ^{17}O,^{14}N, ^{79}Br, and ^{2}H nuclei in crystalline DBNA are influenced by hydrogen/halogen bonding interactions and, as such, are appropriate parameters with which to characterize the properties of these interactions.

References

1. Liu X, Kwan ICM, Wang S, Wu G (2006) G-quartet formation from an N_2-modified guanosine derivative. Org Lett 8:3685–3688
2. Kouvatsos N, Meldrum JK, Searle MS, Thomas NR (2006) Coupling ligand recognition to protein folding in an engineered variant of rabbit ileal lipid binding protein. Chem Commun 4623–4625
3. Černy J, Hobza P (2007) Non-covalent interactions in biomacromolecules. Phys Chem Chem Phys 9:5291–5303
4. Bouchmella K, Dutremez SG, Guérin C, Longato JC, Dahan F (2010) Guanidinium alkynesulfonates with single-layer stacking motif: Interlayer hydrogen bonding between sulfonate anions changes the orientation of the organosulfonate R group from "alternate side" to "same side". Chem Eur J 16:2528–2536
5. Scheiner S (1997) Hydrogen bonding: a theoretical perspective. Oxford University Press, New York
6. Esrafili M, Behzadi H, Hadipour NL (2008) Density functional theory study of N–H···O, O–H···O and C–H···O hydrogen-bonding effects on the 14N and 2H nuclear quadrupole coupling tensors of N-acetyl-valine. Biophys Chem 133:11–18
7. Behzadi H, Esrafili MD, Hadipour NL (2007) A theoretical study of ^{17}O, ^{14}N and ^{2}H nuclear quadrupole coupling tensors in the real crystalline structure of acetaminophen. Chem Phys 333:97–104
8. Grabowski SJ, Sokalski WA, Dyguda E, Leszczyński J (2006) Quantitative classification of covalent and noncovalent H-bonds. Phys Chem B 110:6444–6446
9. Grabowski SJ (2011) What is the covalency of hydrogen bonding? Chem Rev 111:2597–2625
10. Desiraju GR, Steiner T (1999) The weak hydrogen bond in structural chemistry and biology. Oxford University Press, New York
11. Politzer P, Murray JS, Concha MC (2007) Halogen bonding and the design of new materials: organic bromides, chlorides and perhaps even fluorides as donors. J Mol Model 13:643–650
12. Esrafili MD, Hadipour NL (2011) Characteristics and nature of halogen bonds in linear clusters of NCX (X=Cl, and Br): an ab initio, NBO and QTAIM study. Mol Phys 109:2451–2460
13. Duarte DJR, de las Vallejos MM, Peruchena NM (2010) Topological analysis of aromatic halogen/hydrogen bonds by electron charge density and electrostatic potentials. J Mol Model 16:737–748
14. Palusiak M (2010) On the nature of halogen bond—the Kohn–Sham molecular orbital approach. J Mol Struct (THEOCHEM) 945:89–92
15. Bernard-Houplain M-C, Sandorfy C (1973) Low temperature infrared study of hydrogen bonding in dissolved pyrrole and indole. Can J Chem 51:1075–1082
16. Bernard-Houplain M-C, Sandorfy C (1973) A low temperature infrared study of hydrogen bonding in N-Alkylacetamides. Can J Chem 51:3640–3646
17. Rissanen K (2008) Halogen bonded supramolecular complexes and networks. Cryst Eng Commun 10:1107–1113
18. Metrangolo P, Neukirch H, Pilati T, Resnati G (2005) Halogen bonding based recognition processes: a world parallel to hydrogen bonding. Acc Chem Res 38:386–395
19. Metrangolo P, Resnati G (2008) Halogen bonding: fundamentals and applications. Springer, Berlin
20. Ghosh M, Meerts IATM, Cook A, Bergman A, Brouwer A, Johnson LN (2000) Structure of human transthyretin complexed with bromophenols: a new mode of binding. Acta Crystallogr Sect D Biol Crystallogr 56:1085–1095
21. Bertani R, Chaux F, Gleria M, Metrangolo P, Milani R, Pilati T, Resnati G, Sansotera M, Venzo A (2007) Supramolecular rods via halogen bonding-based self-assembly of fluorinated phosphazene nanopillars. Inorg Chim Acta 360:1191–1199
22. Cariati E, Forni A, Biella S, Metrangolo P, Meyer F, Resnati G, Righetto S, Tordin E, Ugo R (2007) Tuning second-order NLO responses through halogen bonding. Chem Commun 2007:2590–2592
23. Brinck T, Murray JS, Politzer P (1993) Molecular surface electrostatic potentials and local ionization energies of Group V–VII hydrides and their anions: Relationships for aqueous and gas-phase acidities. Int J Quantum Chem 48:73–88
24. Auffinger P, Hays FA, Westhof E, Ho PS (2004) Halogen bonds in biological molecules. Proc Natl Acad Sci USA 101:16789–16794
25. Politzer P, Lane P, Concha MC, Ma YG, Murray JS (2007) An overview of halogen bonding. J Mol Model 13:305–311
26. Clark T, Hennemann M, Murray JS, Politzer P (2007) Halogen bonding: the σ-hole. J Mol Model 13:291–296
27. Murray JS, Lane P, Politzer P (2009) Expansion of the σ-hole concept. J Mol Model 15:723–729
28. Murray-Rust P, Motherwell WDS (1979) Computer retrieval and analysis of molecular geometry. 4. Intermolecular interactions. J Am Chem Soc 101:4374–4376
29. Murray-Rust P, Stallings WC, Monti CT, Preston RK, Glusker JP (1983) Intermolecular interactions of the carbon-fluorine bond: the crystallographic environment of fluorinated carboxylic acids and related structures. J Am Chem Soc 105:3206–3214
30. Ramasubbu N, Parthasarathy R, Murray-Rust P (1986) Angular preferences of intermolecular forces around halogen centers: preferred directions of approach of electrophiles and nucleophiles around carbon-halogen bond. J Am Chem Soc 108:4308–4314
31. Politzer P, Murray JS, Concha MC (2008) σ-hole bonding between like atoms; a fallacy of atomic charges. J Mol Model 14:659–665
32. Trogdon G, Murray JS, Concha MC, Politzer P (2007) Molecular surface electrostatic potentials and anesthetic activity. J Mol Mod 13:313–318
33. Awwadi FF, Willett RD, Peterson KA, Twamley B (2006) The nature of halogen···halogen synthons: crystallographic and theoretical studies. Chem Eur J 12:8952–8960
34. Metrangolo P, Murray JS, Pilati T, Politzer P, Resnati G (2011) The fluorine atom as a halogen bond donor, viz. a positive site. Cryst Eng Comm 13:6593–6596
35. Metrangolo P, Murray JS, Pilati T, Politzer P, Resnati G, Terraneo G (2011) Fluorine-centered halogen bonding: a factor in recognition phenomena and reactivity. Cryst Growth Des 11:4238–4246
36. Valerio G, Raos G, Meille SV, Metrangolo P, Resnati G (2000) Halogen bonding in fluoroalkylhalides: a quantum chemical study of increasing fluorine substitution. J Phys Chem A 104:1617–1620
37. Riley KE, Hobza P (2008) Investigations into the nature of halogen bonding including symmetry adapted perturbation theory analyses. J Chem Theory Comput 4:232–242
38. Berski S, Ciunik Z, Drabent K, Latajka Z, Panek J (2004) Dominant role of C−Br···N halogen bond in molecular self-organization. Crystallographic and quantum-chemical study of Schiff-base-containing triazoles. J Phys Chem B 108:12327–12332
39. Esrafili MD, Ahmadi B (2012) A theoretical investigation on the nature of Cl···N and Br···N halogen bonds in F-Ar-X···NCY complexes (X=Cl, Br and Y=H, F, Cl, Br, OH, NH_2, CH_3 and CN). Comput Theor Chem 997:77–82
40. Riley KE, Murray JS, Politzer P, Concha MC, Hobza P (2009) Br ···O complexes as probes of factors affecting halogen bonding: interactions of bromobenzenes and bromopyrimidines with acetone. J Chem Theory Comput 5:155–163

41. Riley KE, Murray JS, Fanfrlík J, Řezáč J, Solá RJ, Concha MC, Ramos FM, Politzer P (2012) Halogen bond tunability II: the varying roles of electrostatic and dispersion contributions to attraction in halogen bonds. J Mol Model. doi:10.1007/s00894-012-1428-x
42. Esrafili MD (2012) Investigation of H-bonding and halogen-bonding effects in dichloroacetic acid: DFT calculations of NQR parameters and QTAIM analysis. J Mol Model. doi:10.1007/s00894-012-1496-y
43. Schmidt MW, Baldridge KK, Boatz JA, Elbert ST, Gordon MS, Jensen JH, Koseki S, Matsunaga N, Nguyen KA, Su SJ, Windus TL, Dupuis M, Montgomery JA (1993) General Atomic and Molecular Electronic Structure System. J Comput Chem 14:1347–1363
44. Bryant R, James SC, Norman NC, Orpen AG (1998) 2,6-Dibromo-4-nitroaniline. Acta Cryst C 54:1113–1115
45. Zhao Y, Schultz NE, Truhlar DG (2005) Exchange-correlation functional with broad accuracy for metallic and nonmetallic compounds, kinetics, and noncovalent interactions. J Chem Phys 123:161103
46. Zhao Y, Schultz NE, Truhlar DG (2006) Design of density functionals by combining the method of constraint satisfaction with parametrization for thermochemistry, thermochemical kinetics, and noncovalent interactions. J Chem Theory Comput 2:364–382
47. Zhao Y, Truhlar DG (2006) A new local density functional for main-group thermochemistry, transition metal bonding, thermochemical kinetics, and noncovalent interactions. J Chem Phys 125:194101
48. Zhao Y, Truhlar DG (2008) The M06 suite of density functionals for main group thermochemistry, thermochemical kinetics, noncovalent interactions, excited states, and transition elements: two new functionals and systematic testing of four M06-class functionals and 12 other functional. Theor Chem Acc 120:215–241
49. Zhao Y, Truhlar DG (2007) Density functionals for noncovalent interaction energies of biological importance. J Chem Theory Comput 3:289–300
50. Gu JD, Wang J, Leszczynski J, Xie YM, Schaefer HF (2008) To stack or not to stack: performance of a new density functional for the uracil and thymine dimers. Chem Phys Lett 459:164–166
51. Bulat FA, Toro-Labbe A, Brinck T, Murray JS, Politzer P (2010) Quantitative analysis of molecular surfaces: areas, volumes, electrostatic potentials and average local ionization energies. J Mol Model 16:1679–1691
52. Bader RFW (1990) Atoms in molecules-a quantum theory. Oxford University Press, New York
53. Biegler-Konig F, Schonbohm J, Bayles D (2001) AIM 2000. J Comput Chem 22:545–559
54. Jeziorski B, Moszynski R, Szalewicz K (1994) Perturbation theory approach to intermolecular potential energy surfaces of Van der Waals complexes. Chem Rev 94:1887–1930
55. Dalton, a molecular electronic structure program, Release 2.0 (2005) http://www.kjemi.uio.no/software/dalton/dalton.html
56. Bukowski R, Cencek W, Jankowski P, Jeziorski B, Jeziorska M, Kucharski SA, Lotrich VF, Misquitta AJ, Moszynski R, Patkowski K, Podeszwa R, Rybak S, Szalewicz K, Williams HL, Wheatley RJ, Wormer PES, Żuchowski PS (2008) SAPT2008: "An ab initio program for many-body symmetry-adapted perturbation theory calculations of intermolecular interaction energies" by sequential and parallel versions; University of Delaware and University of Warsaw; http://www.physics.udel.edu/_szalewic/SAPT/SAPT.html
57. Cukras J, Sadlej J (2008) Symmetry-adapted perturbation theory interaction energy decomposition for some noble gas complexes. Chem Phys Lett 459:44–48
58. Lucken EAC (1990) Nuclear quadrupole coupling constants. Academic, London
59. Pyykkö P (2001) Spectroscopic nuclear quadrupole moment. Mol Phys 99:1617–1629
60. Stewart RF (1972) Valence structure from X–ray diffraction data: physical properties. J Chem Phys 57:1664–1668
61. Hirschfelder JO, Curtiss CF, Bird RB (1954) Molecular theory of gases and liquids. Wiley, New York
62. Bader RFW, Carroll MT, Cheeseman JR, Chang C (1987) Properties of atoms in molecules: atomic volumes. J Am Chem Soc 109:7968–7979
63. Bondi A (1964) van der Waals volumes and radii. J Phys Chem 68:441–451
64. Vener MV, Manaev AV, Egorova AN, Tsirelson VG (2007) QTAIM study of strong H-bonds with the O−H···A fragment (A=O, N) in three-dimensional periodical crystals. J Phys Chem A 111:1155–1162
65. LaPointe SM, Farrag S, Bohórquez HJ, Boyd RJ (2009) QTAIM study of an α-helix hydrogen bond network. J Phys Chem B 113:10957–10964
66. Rozas I, Alkorta I, Elguero J (2000) Behaviour of ylides containing N, O and C atoms as hydrogen bond acceptors. J Am Chem Soc 122:11154–11161
67. Esrafili MD, Beheshtian J, Hadipour NL (2011) Computational study on the characteristics of the interaction in linear urea clusters. Int J Quantum Chem 111:3184–3195
68. Panek JJ, Jezierska A (2007) Symmetry-adapted perturbation theory analysis of the N···HX hydrogen bonds. J Phys Chem A 111:650–655
69. Boys SF, Bernardi F (1970) The calculation of small molecular interactions by the differences of separate total energies. Some procedures with reduced errors. Mol Phys 19:553–566
70. Jaffe RL, Smith GD (1996) A quantum chemistry study of benzene dimer. J Chem Phys 105:2780–2788
71. Esrafili MD (2012) Characteristics and nature of the intermolecular interactions in boron-bonded complexes with carbene as electron donor: an ab initio, SAPT and QTAIM study. J Mol Model 18:2003–2011
72. Song H-J, Xiao H-M, Dong H-S (2006) Theoretical study of properties of H-bonds and intermolecular interactions in linear cis-, trans-cyclotriazane clusters (n=2–8). J Chem Phys 124:74317
73. Politzer P, Riley KE, Bulat FA, Murray JS (2012) Perspectives on halogen bonding and other r-hole interactions: Lex parsimoniae (Occam's Razor). Comput Theor Chem 998:2–8
74. Yim CT, Whitehead MA, Lo DH (1968) The chemical interpretation and the temperature dependence of the ^{14}N nuclear quadrupole resonance of aniline and several derivatives. Can J Chem 46:3594–3604
75. Rabbani SR, Edmonds DT, Gosling P (1987) Nuclear quadrupole resonance of ^{14}N and ^{2}H in pyrimidines, purines, and their nucleosides. J Magn Reson 72:422–433